A HYBRID GWO-RBFNN MODEL FOR INTER-TURN INSULATION FAULT DETECTION AND DIAGNOSIS IN INDUCTION MOTOR

1.**Gopu Venugopal**
Sri Ramakrishna Engineering College, Coimbatore
gopuslm@yahoo.co.in

2.Gopalakrishnan Varadarajan
Government College of Technology, Coimbatore
gopalakrishnan.v@gct.ac.in

Abstract-*This paper proposes an optimal detection and classification of inter-turn insulation faults in the induction motor (IM) using a hybrid optimization technique. The proposed hybrid optimization technique is the joined execution of both the Grey Wolf Optimization Algorithm (GWOA) and Radial Basis Function Neural Network (RBFNN) and in this way, it is named as GWO-RBFNN technique. The required fault training dataset is gathered through the client characterized framework show through the proposed GWO algorithm. In the proposed approach, RBFNN is utilized in two phases with the end goal of detection of the inter-turn insulation faults. The ordinary RBFNN first phase is utilized to recognize the motors healthy or unhealthy condition under various situations. The second phase of the RBFNN is playing out the classification of the unhealthy condition of motors to distinguish the correct inter-turn faults for protection. Here, the second phase RBFNN learning procedure is enhanced by using the GWOA in perspective of the minimum error objective function. The proposed GWO-RBFNN method plays an evaluation process to protect the induction machine and detect the fault in the IM at the inception stage. The proposed GWO-RBFNN technique guarantees the system with lessens complexity for the detection and classification of the inter-turn insulation fault and hence the accuracy of the system is raised. The proposed model is executed in MATLAB/Simulink working stage and the execution is assessed with the current procedures.*

Keywords: *Induction motor, Inter-turn insulation faults, Grey wolf optimization algorithm, Radial basis function neural network, motors healthy or unhealthy condition.*

1. Introduction

These days, for the protected and proficient running of mechanical plants and procedures, the electric motors assume a significant job [1]. The costly failures in the motors are kept away from by the early discovery of variations from the norm [2]. The greater parts of the studies are utilized to find the failure in squirrel-cage motors, bearing-and stator-winding-related inadequacies. Additionally, it shows that most of stator winding failures of motor result from turn-to-turn insulation breakdown [3]. In spite of the fact that, to show the time delay between inter-turn and ground wall insulation failures there is no exploratory information is utilized, it is plausible that the progress between the two states isn't immediate. To neighboring the coils and the stator core, decreasing fix cost and motor blackout time, early identification of inter-turn shorts amid motor activity would dispose of ensuing harm [4]. The nearness of a shorted turn is shown by the presently existed instrumentation, yet just with the motor expelled from the administration. In the event that these faults are left undetected, they will inevitably deteriorate into a machine failure [5]. At the point when the failure of machine happens, it might be harmed by close personnel. Additionally, there is a generous cost related to vacation and fizzled machine fix. As such, at the beginning stage, it is always appealing to blame recognizes [6]. To distinguish the bearing, stator, and eccentricity-related deficiencies, an explicit mathematical model is used by the model-based fault detection and diagnosis strategies [7]. The vast majority of the examination broke down the different FAULT location techniques, for example, Motor Current Signature Analysis (MCSA), Axial Flux-Based Methods, Vibration Analysis, and so on.

In the IM, asymmetry in the machine impedance is happened by both Modeling and Experimentation that the winding insulation faults to draw unbalanced phase currents [8]. Because of this unbalance, the negative sequence currents streaming in the line. Be that as it may, voltage unbalance, machine saturation, and so on is caused the negative sequence currents [9]. A number of time-frequency domain systems have been proposed including Short-Time Fourier Transform (STFT), Wigner Ville Distribution (WVD), and Wavelet Transform (WT) in the ongoing writing. To identify bearing deformities, the greater part of the scientists used the stator current by means of wavelet packet decomposition [10-12]. The recently referenced frequency-domain approaches require the bearing defect frequencies to be known or pre-assessed. The other insufficiency is the extending inconvenience in researching the vibration spectrum when the signal-to-

noise ratio is low. If the vibration spectrum has an expansive number of frequency segments it results in the multifaceted nature of the system [13-16]. Using a reasonable, solid, and non-obtrusive system Artificial Neural Network (ANN) has the limit of grasping the motor checking and fault identification issue. In any case, the fault discovery process does not give heuristic thinking [17-19]. On the other hand, fuzzy logic can give heuristic thinking, yet difficult to give precise solutions [20].

In the paper, a combined strategy of GWO-RBFNN for detection and classification of inter-turn insulation fault in IM is proposed. The motivation behind the proposed technique is to detect and classify the inter-turn insulation fault exhibited in the IM under healthy and unhealthy conditions. The remaining section of the paper is organized as follows. Section 2 delineates the recent research works about the inter-turn faults in the IM. Section 3 includes the analytic modeling of an induction motor under stator inter-turn fault; section 4 delineates the proposed inter-turn insulation faults diagnosis method in induction motor; section 5 and 6 includes the simulation analysis and conclusions

2. Recent Research Works: A Brief Review

Numerous research works have previously existed in the literature which was based on the detection of inter-turn faults in the IM using various techniques and various aspects. Some of the works are reviewed here.

For the fault diagnosis in the IM, practical machine learning based fault diagnosis strategy was proposed by M. Ali et al. [21]. For feature extraction, the authors have utilized the two signal processing techniques such as matching pursuit(MP) And discrete wavelet transform(DWT). For IM's fault diagnosis, three classification algorithms, support vector machine(SVM), K-nearest neighbors(KNN), and ensemble, with 17 different classifiers are utilized. To compute features for a specific fault a novel curve fitting procedure was created. For incipient fault diagnosis of the synchronous generator, a consolidated system of Moth– Flame Optimization (MFO) algorithm and Fuzzy Logic Controller(FLC) was displayed by V. Boorgula et al. [22]. The inspiration for their work was different fault location under healthy and unhealthy conditions. In their methodology, the MFO was utilized to gather the data-set from the input current signal. The FLC was utilized to diagnose the faults subject to the dataset. So as to assess the adequacy of the proposed technique, the incipient faults are dissected.

For inverter-fed IM stator faults location under closed-loop control, an efficient methodology was proposed by E. Elbouchikhi et al. [23]. The symmetrical components (SCS) of the stator currents were utilized to the proposed conclusion approach. The maximum likelihood estimator (MLE) was utilized to assess the supply fundamental frequency and the three-phase phasors. For unbalance fault detection, authors have utilized the Generalized Likelihood Ratio Test (GLRT) strategy. In three-phase IMs, the level of stator winding shorted turns was identified by neural networks as a productive diagnostic tool which was exhibited by L. Maraaba et al. [24]. For the plan and training of the neural network, the mean, variance, max, min, and F120 time dependent on factual and frequency-related highlights were observed to be exceptionally particular for connecting the caught electromechanical torque with its comparing level of shorted turns.

To distinguish incipient stator winding inter-turn short-circuits in IM, P. Rebouças Filho et al. [25] have contributed a solid methodology. Various sorts of short-circuit in the generator was distinguished utilizing a wind turbine test-bench. To fabricate a fault database, the electrical current was gained. Here, the utilization of four feature extraction systems with three classifiers was utilized. For IM fault recognition, a novel radial flux sensing technique was shown by G. Surya et al. [26]. Serious research endeavors in the past have been centered around the flux signature analysis as they have been increasingly proficient contrasted with classical motor current signature analysis (MCSA).

2.1. Motivation for the Research Work

The review of the ongoing research work shows that the detection of inter-turn insulation failure in the IM is a basic contributing part. In a mechanical plant, broad amounts of electrical drives are presented. Along these lines, in such an establishment the strength of individual motors detection is huge. Diagnostics of fault is basic for keeping up a key separation from the cataclysmic impacts, for instance, unexpected failure of electric drive systems. Thusly, in the recognition of variations from the norm in motor a precise demonstrating of motors is the underlying advance. In light of the composition, distinctive fault identification procedures, for instance, neural networks (NNS), Generalized Likelihood Ratio Test (GLRT), Fast Fourier Transform (FFT), ETC. ANN has the limit of disentangling the observing and fault recognition issue of the motor in any case in the fault identification process it doesn't give the heuristic method. Regardless, in veritable applications, the genuine weaknesses of artificial intelligence (AI) procedures are black-box data processing structure and high computational cost. Furthermore, for different state conditions, the underlying training stage is an issue since it requires an extensive arrangement of stator currents database. For optimal operation, this stage is

essential and may be conveyed limited game plan of systems. Nevertheless, one of the issues with FFT analysis and other frequency-domain approaches require the frequencies of bearing deformity be known or pre-evaluated. The other deficiency when the signal-to-noise ratio is low there is the extending inconvenience in separating the vibration spectrum and when the signal-to-noise ratio is high then the vibration spectrum has innumerable parts. Regardless of the way that the above techniques are used for foreseeing the inter-turn faults, the algorithm unpredictability is high a direct result of an extended number of tests required. To vanquish these troubles, an optimal detection, and classification of faults using trendsetting innovation. In related works, few control methods are shown to identify and classify the inter-turn faults; the recently referenced confinements have roused to do this examination work.

3. Analytic Modeling of Induction Motor under Stator Inter-Turn Fault

3.1. Operating Principles of Induction Motor

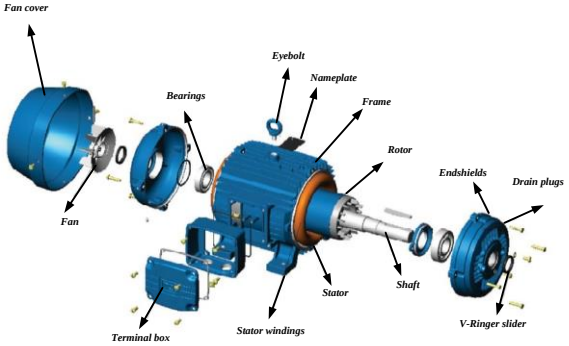

Figure 1: Operating Principles of Induction Motor

The IMs involves the most significant spot in the protected and effective running of industrial plants and processes. In this motor, a rotating magnetic field is rendered by a three-phase power supply. The magnetic field offered in the IM is generated by the AC power provided to the stator of the motor that rotates in time with the AC oscillations. A rotor of the IM pivots at a slower speed than the stator field while synchronous rotor of the motor turns at a similar rate as the stator field. Hence, the magnetic field of the stator in the IM is changing or rotating with respect to the rotor. This invigorates the inverse current in the rotor of the IM; accordingly, the secondary winding of the motor is short-circuited or shut through outside impedance. The currents in the windings of the rotor actuated by the rotating magnetic flux and the currents incited in secondary windings of the transformer both are comparative. In the rotor, the magnetic fields are made by the currents in the rotor windings which respond against the stator field. The rotating stator magnetic field because of the reason for induced current in the rotor windings inverse the change in currents of the rotor-windings; the rotor will begin to rotate toward the rotating stator magnetic field [27]. The rotor will accelerate until the connected load is adjusted by the magnitude of induced rotor current and torque. The operation of the IM is slower than synchronous speed because of the nonappearance of induced rotor current since the rotation at synchronous speed. Subsequently, the mathematical formulation of the IM is depicted in the accompanying section.

3.1.1 Mathematical Modeling of Induction Motor

The mathematical model of the IM is formulated through the equivalent circuit developing of the IM. The equivalent circuit is modeled subject to the integrated structure of the stator and rotor circuit model. The stator circuit model is illustrated in figure 2(a), a flux $\emptyset m$ is step up when a voltage V_1 is applied to stator terminals. Along these lines, the electromagnetic flux (e.m.f) in the stator winding is induced by this flux. In the stator winding, the voltage drops I_1r_1 and I_1x_1 caused by the flow of current I_1. The motor equation is estimated subject to the E_1, V_1, $I_1r_1$and I_1x_1. The rotor circuit models are illustrated in figure 2 (b and c). In this rotor circuit, an e.m.f sE_2 and flow of current I_2 both are actuated by the mutual flux $\emptyset_m$. The rotor resistance and leakage reactance both are represented as r_2 and x_2 at standstill (i.e. s =1). The leakage inductance sx_2 is generated when the motor is operating at slip s which is shown in figure 2(b). Though, the elective rotor circuit model with mechanical load is illustrated in figure 2(c) and the line frequency current in this model is represented as I_2 [28].

The input 3-phase power supplied to an IM is estimated as follows,

$$P_i = 3V_1 I_1 \cos\theta_1 \quad (1)$$

Where the per phase value of the stator voltage is denoted as V_1, as well as per phase values of the current and stator power are represented as I_1 and cosθ respectively. A portion of this power is involved in stator core losses and stator copper losses.

Stator copper losses is given by

$$P_{cu} = 3I_1^2 r_1 \quad (2)$$

$$P_g = P_i - P_{cu} \quad (3)$$

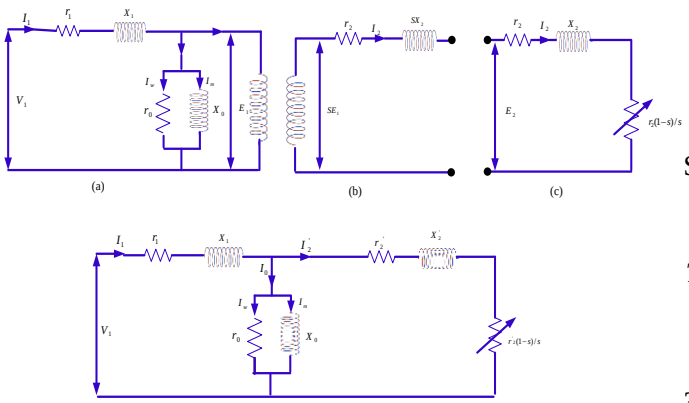

Figure 2: Development of equivalent circuit of 3-phase IM (a) stator circuit model (b) and (c) rotor models (d) complete equivalent circuit model

Where the power transferred across the air gap to the rotor is represented as P_g. Here, the mechanical power is developed and P_m is obtained after rotor copper losses are subtracted from P_g. A part from Pm of power output $P_o$is consumed as friction and windage and stray losses and the remainder is the power output P_o.

$$P_g = 3E_2 I_2 \cos\theta_2 = \frac{3I_2^2 r_2}{s} \tag{4}$$

Also,

$$P_g = 3E_2 I_2^{'} \cos\theta_2 = \frac{3I_2^{'2} r_2^{'}}{s} \tag{5}$$

The rotor copper-loss is estimated as follows,

$$P_{cu} = 3I_1^2 r_1 = 3I_2^{'2} r_2^{'} \tag{6}$$

The Rotor Copper-loss = sP_g is estimated from the equations (4) and (6),

$$P_m = P_g - Rotor\ copperloss = P_g(1-s) \tag{7}$$

$$P_o = P_m - Friction,\ windage\ and\ stray\ losses = P_g(1-s) \tag{8}$$

The frequency of rotor current is low. In this manner, power loss is very small and thus negligible. In the motor, the electromechanical power conversion process developed the mechanical power which is used to generate the torque T.

Thus,

$$T = \frac{P_m}{\omega_m} = \frac{P_m}{2\pi n} \quad \text{Or} \quad T = \frac{3I_2^{'2} r_2^{'}}{2\pi n}\left[\frac{1-s}{s}\right] \tag{9}$$

In the above equation, $n = n_s(1-s)$

The torque developed is proportional to the air gap power Pg. The torque estimated in synchronous watts is known as the air gap power Pg. The torque developed is acquired from this, if this power is partitioned by synchronous angular velocity $2\pi ns$. It very well may be determined from the following equation,

$$I_2^{'} = \frac{V_1}{\left[\left(r_1 + \frac{r_2^{'}}{s}\right)^2 + \left(x_1 + x_2^{'}\right)^2\right]^{0.5}} \tag{10}$$

Substitute equation (10) in equation (11),

$$T = \left[\frac{3}{2\pi n_s}\right]\left[\frac{r_2^{'}}{s}\right]\left[\frac{V_1^2}{\left(r_1 + \frac{r_2^{'}}{s}\right)^2 + \left(x_1 + x_2^{'}\right)^2}\right] \tag{11}$$

3.2. Formulation of Induction Motor with Stator Inter-Turn Insulation Faults

In the IM, the stator inter-turn insulation fault is considered as one of the possible frequently happened causes among the types of faults in the stator. This type of stator defect is causes during the gathering of stator coils in the assembling process which causes the low quality of the material or errors, due to these errors the faults occurred in the inter-turn insulation. Besides, when the motor is inactivity or maintenance is available, there might be a defect happened in inter-turn insulation. The inter-turn insulation faults can begin imperceptible, nonetheless, during the motor life expectancy; this can build up a short among a few turns of a similar phase or even extraordinary phases. The decision might be probably not going to be conceivable, for example lack of phase; short circuit between phases; short circuit involving earth [25]. In this section, the mathematical model used for simulating IMs under stator inter-turn insulation faults is presented. The fault occurred in phase-a as illustrated in figure 3 is considered to derive the model.

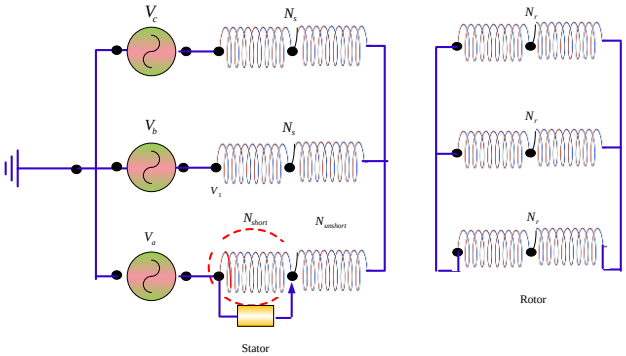

Figure 3: Induction Motor with Inter-Turns Circuit Diagram

$$N_s = N_{short} + N_{un-short} \tag{12}$$

In the above equation, the number of turns per phase of the stator and rotor is represented as N_s and N_r. The number of shorted and un-shorted turns is represented as N_{short} and $N_{un-short}$. Here, as the coil's resistance is directly proportional to the number of turns in the coil.

The resistance of the shorted and un-shorted parts of the phases in the stator is estimated using the following equation,

$$r_{shor} = \frac{N_{short}}{N_s = \mu r_s} \quad (13)$$

$$r_{un-short} = (1-\mu)\, r_s \quad (14)$$

Where the percentage of shorted turns is represented as μ, the stator resistance per phase is denoted as r_s. Besides, since the relation between the inductance and the number of turns is squared, motor inductance needs to be modified. The mathematical equations for the inductance motor under stator inter-turn insulation fault are given in the following section.

$$\varphi_q^{short} = \int \left(V_q^{short} - r_{short} I_q^{short}\right) \quad (15)$$

$$\varphi_q^s = \int \left(V_q^s - V_q^{short} - r_{11}^s i_q^s - r_{12}^s i_d^s\right) dt \quad (16)$$

$$\varphi_d^s = \int \left(V_d^s - r_{21}^s i_q^s - r_{22}^s i_d^s\right) dt \quad (17)$$

$$\varphi_q^r = \int \left(\omega_r \varphi_d^r - r_r i_q^r\right) dt \quad (18)$$

$$\varphi_d^r = \int \left(\omega_r \varphi_q^r - r_r i_d^r\right) dt \quad (19)$$

$$r_{sqd0} = \begin{bmatrix} r_{11}^s & r_{12}^s & r_{13}^s \\ r_{21}^s & r_{22}^s & r_{23}^s \\ r_{31}^s & r_{32}^s & r_{33}^s \end{bmatrix} \quad (20)$$

where the stator qd0 voltages are denoted as V_q^s, V_d^s and V_o^s respectively; the shorted winding voltage is represented as V_q^{short}; the stator qd0 currents are denoted as I_q^s, I_d^s and I_o^s respectively; I_q^r, I_d^r and I_o^r are stator qd0 current referring to the stator side, respectively; the equivalent rotor resistance per phase is denoted as r_r; the stator qd linkage fluxes are expressed as φ_q^s and φ_d^s respectively; φ_q^r and φ_d^r are rotor qd linkage fluxes; the linkage flux for the shorted turns is denoted as φ_q^{short}; ω_r is the rotor speed; and r_{sqd0} is the stator resistance matrix in the qd0 frame. In the qd0 frame, the flux current is formulated using the following equation,

$$\begin{bmatrix} \varphi_q^{short} \\ \varphi_q^s \\ \varphi_d^s \\ \varphi_q^r \\ \varphi_d^r \end{bmatrix} = \begin{bmatrix} L_q^{short} & L_q^{sshort} & 0 & L_q^{rshort} & 0 \\ L_q^{sshort} & L_q^s & 0 & L_q^{sr} & 0 \\ 0 & 0 & L_d^s & 0 & L_d^{sr} \\ L_q^{rshort} & L_q^{sr} & 0 & L_q^r & 0 \\ 0 & 0 & L_d^{sr} & 0 & L_d^r \end{bmatrix} \begin{bmatrix} I_q^{short} \\ I_q^s \\ I_d^s \\ I_q^r \\ I_d^r \end{bmatrix} \quad (21)$$

Where,

$$L_d^s = L_{\sigma s} + \frac{3}{2} L_m \quad (22)$$

$$L_q^s = \frac{2}{3}\left((1-\mu)^2\left(L_{\sigma s} + \frac{3}{2}L_m\right) + \frac{1}{2}\left(L_{\sigma s} + \frac{3}{2}L_m - \frac{1}{2}L_m\right) + (1-\mu)L_m\right) \quad (23)$$

$$L_q^{sshort} = \frac{2}{3}\left(\mu(1-\mu)L_m + \frac{\mu}{2}L_m\right) \quad (24)$$

$$L_q^{short} = \frac{2}{3}\left(\mu^2\left(L_{\sigma s} + \frac{3}{2}L_m\right)\right) \quad (25)$$

$$L_{srqd0} = \begin{bmatrix} \left(\frac{L_m}{2} + \frac{L_m N_{us}}{N_s}\right) + \frac{L_m N_{short}}{2N_s} & 0 & 0 \\ 0 & \frac{3L_m}{2} & 0 \\ \left(-\frac{L_m}{2} + \frac{L_m N_{us}}{2N_s}\right) + \frac{L_m N_{short}}{2N_s} & 0 & 0 \end{bmatrix} = \begin{bmatrix} L_q^{sr} + L_q^{rshort} & 0 & 0 \\ 0 & L_d^r & 0 \\ L_{31}^{sr} & 0 & 0 \end{bmatrix} \quad (26)$$

Where L_m is the mutual inductance; $L_{\sigma s}$ is the stator leakage inductance per phase; $L_{\sigma r}$ is the rotor leakage inductance per phase; L_{rd} is the rotor d-axis inductance and L_{rq} is the rotor q-axis inductance. The mechanical speed and electromagnetic torque are expressed in Equation (27):

$$\omega_r(t) = \frac{P}{2} \int \left(T_{em} + T_{mech} - T_{damp}\right) dt \quad (27)$$

$$T_{em} = \frac{3P}{4}\left(\varphi_d^s I_q^s - \varphi_q^s I_d^s\right) \quad (28)$$

Where T_{em} is the electromagnetic torque; T_{mech} is the load torque; T_{damp} is the damping torque; J is the motor inertia; and $\omega_r(t)$ is the rotor speed.

4. Proposed Inter-Turn Insulation Faults Diagnosis Method in Induction Motor

The proposed method for detection and diagnosis of inter-turn insulation fault in the IM is illustrated in figure 1. The main goal of the proposed approach is to detect and diagnose the inter-turn insulation fault in the IM while the variety of electrical characteristics, for example, voltage, current, torque, and speed. In this paper, the proposed approach is the combined execution of both the GWO and RBFNN; due to this combination, the proposed approach is called a GWO-RBFNN technique. Here, the proposed method has two stages, for detecting and diagnosing inter-turn insulation fault in the IM. In the initial stage, the required fault training dataset gathered by the GWO algorithm as well as the first phase of the RBFNN is used to detect and recognize the healthy and unhealthy motors under various conditions whereas the second phase of the RBFNN is used to detect the correct inter-turn faults for protection. The proposed GWO-RBFNN method plays an evaluation process to protect the IM and detect the fault in the IM at the inception stage**.** The

proposed GWO-RBFNN technique guarantees the system with lessens complexity for the detection and classification of the inter-turn insulation fault and hence the accuracy of the system is raised. The detailed description of the proposed GWO-RBFNN approach is delineated in the following section.

4.1. GWO Algorithm for Fault Dataset Generation

The GWO algorithm is one of the latest bio-inspired algorithms which mimics the leadership hierarchy and hunting mechanism of grey wolves in nature is proposed in [29]. The grey wolf behavior is stimulated to live in a pack which is the main concept of this algorithm. They have a serious social dominant hierarchy. The leadership hierarchy is stimulated by the four types of grey wolves' alpha (α), beta (β), delta (δ), and omega (ω). The fittest solution of α is used to design the mathematical formulation of the social hierarchy of wolves while designing GWO. Consequently, the β and δ are considered to determine the second and third best solutions respectively. The rest of the candidate solutions are assumed to be omega (ω) [30]. Figure 5 shows the hunting behavior of grey GWO algorithm. In the proposed approach, the GWO algorithm is used to generate the datasets of fault signals to identify healthy and unhealthy motors. The step by step process of the GWO algorithm is delineated in the following section.

Step by step process of GWO

Step 1: Initialization and Random generation

(Encircling prey)

In the initialization process, the Grey wolves are encircling the prey during the hunting process. In the proposed approach, the power values and the system constraints such as voltage speed and torque are initialized [31]. The following equations are formulated in order to randomly generate the initialized parameters (encircling behavior).

$$\vec{P}(t+1) = \vec{P}_p(t) - \vec{A} \,.\, \vec{D} \tag{29}$$

$$\vec{D} = \left| \vec{C}.\vec{P}_p(t) - \vec{P}(t) \right| \tag{30}$$

Where t is the iteration number, $\vec{P}$ is the random generation of power with respect to time during the occurrence of the fault. The vectors $\vec{A}$ and $\vec{C}$ are computed by the following equation,

$$\vec{A} = 2a. \,.\, \vec{R}_1 - a \tag{31}$$

$$\vec{C} = 2\vec{R}_2 \tag{32}$$

Where the randomly generated vectors $\vec{R}_1$ and $\vec{R}_2$ are generated between the range of [0, 1] and in the overall iterations, the value is decreased from 2 to 0. The vector $\vec{C}$ is generated between the ranges of [0, 2]. These ranges are used to compute the fitness solution.

Step 2: Fitness function Evaluation (Hunting)

The possible fitness solutions (possible location of prey) are mathematically obtained by the alpha (α), beta (β), and delta (δ).

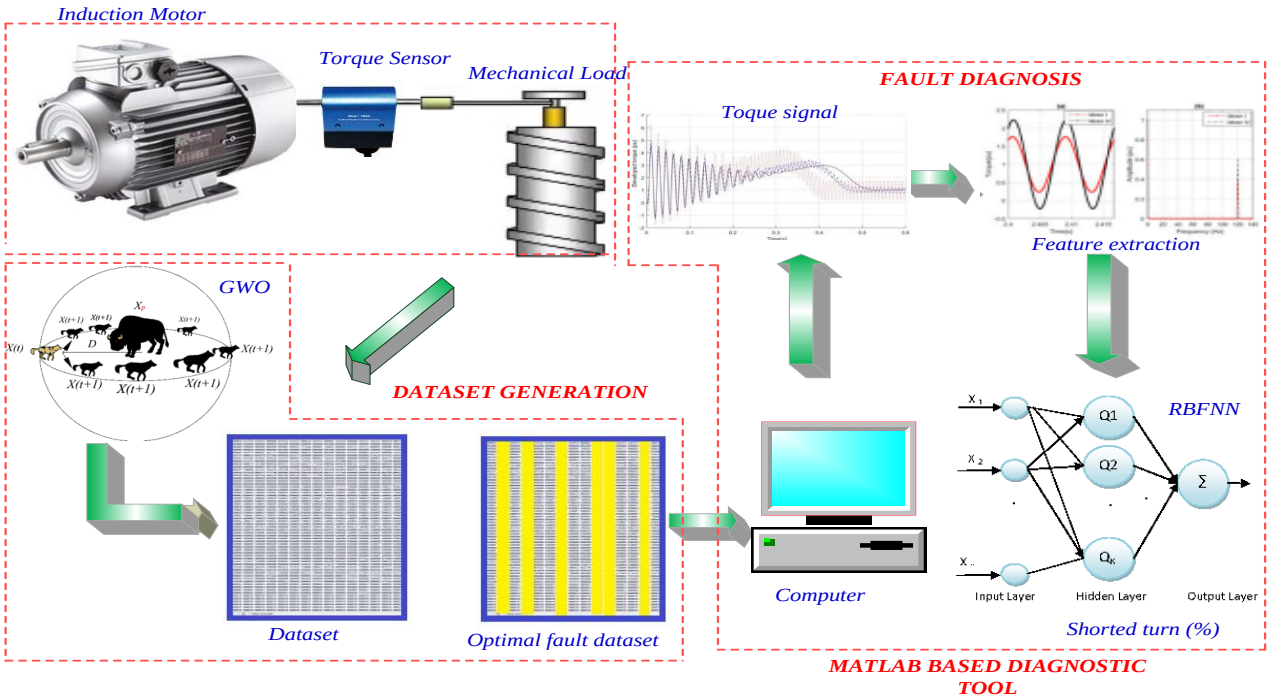

Figure 4: Proposed method for inter-turn faults diagnosis in induction motor

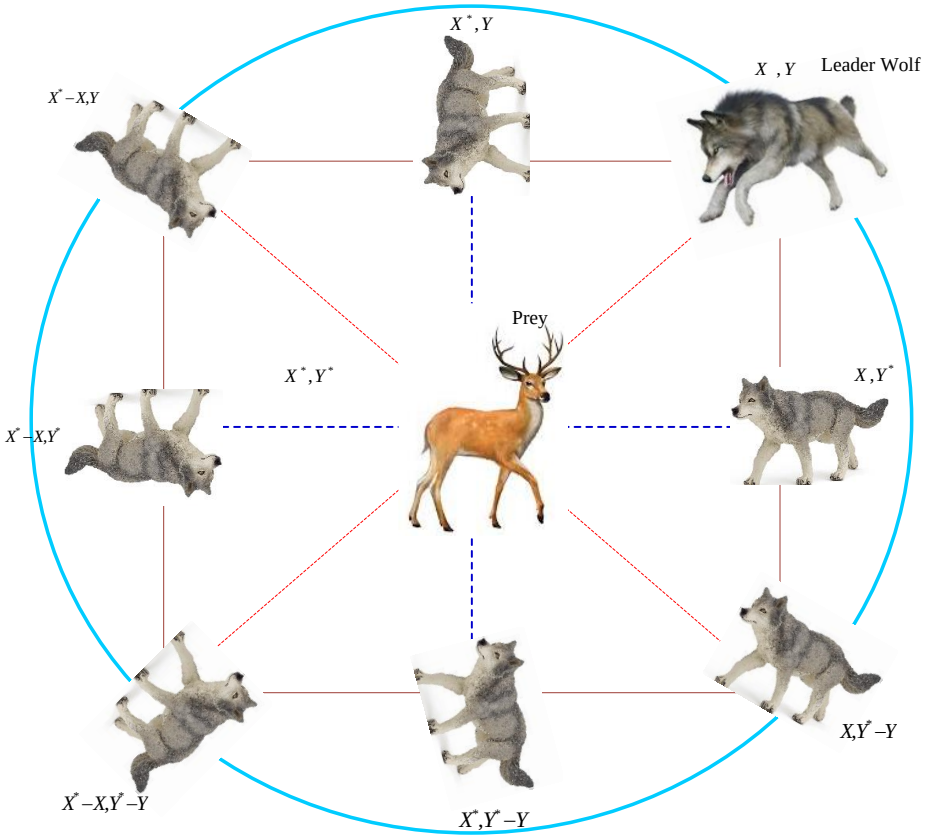

Figure 5: Hunting behaviour of grey wolves

According to the best solution, the initial three solutions are obtained so far and force the other search agents to update the best solution [32]. The objective function of the proposed approach is given as follows,

$$\vec{P}(t+1) = \frac{\vec{P}_1 + \vec{P}_2 + \vec{P}_3}{3} \quad (33)$$

$$\vec{P}_i = \min \{P_{tar}(t) - P(t)\} \quad (34)$$

$$Subject\ to \begin{cases} V_{abci}^{\min}(t) \le V_{abi}(t) \le V_{abci}^{\max}(t) \\ \omega^{\min}(t) \le \omega(t) \le \omega^{\max}(t) \\ T^{\min}(t) \le T(t) \le T^{\max}(t) \end{cases} \quad (35)$$

Where, $P_{tar}(t)$ and $P(t)$ are the target and the actual power signal of IM, $V_{abi}(t)$ is the voltage at three-phase fault at the time t, $\omega(t)$ denotes the speed of the IM at time t and torque produced at a time t is represented as $T(t)$.

Step 3: Updating

The final best solution a is updated in this step. The tradeoff between exploration and exploitation are controlled by the parameter a, that is linearly updated to range from 2 to 0 in each iteration which is estimated using the following equation [33],

$$a = 2 - t\frac{2}{Max\ iter} \quad (36)$$

Where t is the iteration number and Max iter is the total number of iteration.

Step 3: Termination

After completing the process of the GWO technique, the dataset is determined. Once the process is completed, the healthy and unhealthy motors are identified subject to these datasets using the RBFNN technique. The detailed description of the RBFNN is delineated in the following section.

4.2. Detection of the healthy and unhealthy motor using RBFNN

The RBFNN is an artificial neural network that uses radial basis functions as activation functions. The RBFNN basically have three layers such as an input layer, a hidden layer with a radial basis function (RBF) activation function and an output layer. A vector of real numbers is considered as the input of RBFNN. The inputs of RBF and neuron parameters are linearly combined to form the output of the network. RBFNN have many uses, including function approximation, time series prediction, classification, and system control [34]. In the proposed approach, the RBFNN is used to generate the diagnosis of the performance of the IM. Figure 6 shows the structure of the RBFNN.

The step by step process of the RBFNN is delineated in the following section.

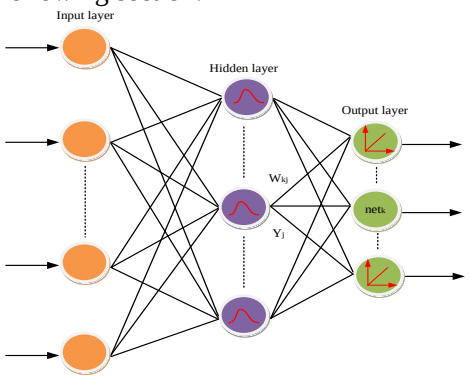

Figure 6: Structure of RBFNN

Step by step process of RBFNN

Step 1: In this step, the weights of all the neurons are initialized; (i.e) squared error (SE), and the deviation of error *DSE(t)*.

Step 2: The accompanying formulation is used to determine the backpropagation error (BPR) of the target.

$$SE_{BP}^{k} = N^{k}(tar) - N^{k}(out) \qquad (37)$$

Where, $N^{k}(tar)$ is the network target of the k-th node and $N^{k}(out)$ is the current output of the k-th node

Step 3: The current output of the network is computed in this step using the following equation [35],

$$N^{k}(out) = f\left(N^{k}(n)\right) + \sum_{n=1}^{L} w_{kn} N^{k}(n) \qquad (38)$$

$$N^{k}(n) = \frac{1}{1+\exp\left(-w_{kn}N^{k} - w_{in}N^{1}\right)} \qquad (39)$$

The bias function of the radial bias function is computed as follows,

$$f\left(N^{k}(n)\right) = \sum_{n=1}^{L} w_{kn} H_{k}\left(f\left(N^{k}(n)\right)\right) \qquad (40)$$

The k-th neuron of the hidden layer is computed as follows,

$$H_{k}\left(f\left(N^{k}(n)\right)\right) = \exp\left(\frac{-\left\|\left(N^{k}(n)\right) - C_{p}\right\|^{2}}{r_{p}}\right) \qquad (41)$$

Where, $N^{k}(n)$ is the bias function of the node k, w_{kn} is the weight of the k-th neuron, $H_{k}\left(f\left(N^{k}(n)\right)\right)$ is the response of the k-th neuron of the hidden layer, C_{p} is the center value of the p-th neuron, r_{p} is the scalar factor [36].

Step 4: This step computes the new best solution for all the neurons which given as follows,

$$W_{new} = W_{old} + \Delta W \qquad (42)$$

In the above equation, $\Delta W = \xi N^{k}(n) SE_{BP}^{k}$, W_{old} is the earlier weight, ΔW is the difference in weight, $\xi N^{k}(n) SE_{BP}^{k}$ is the Learning rate.

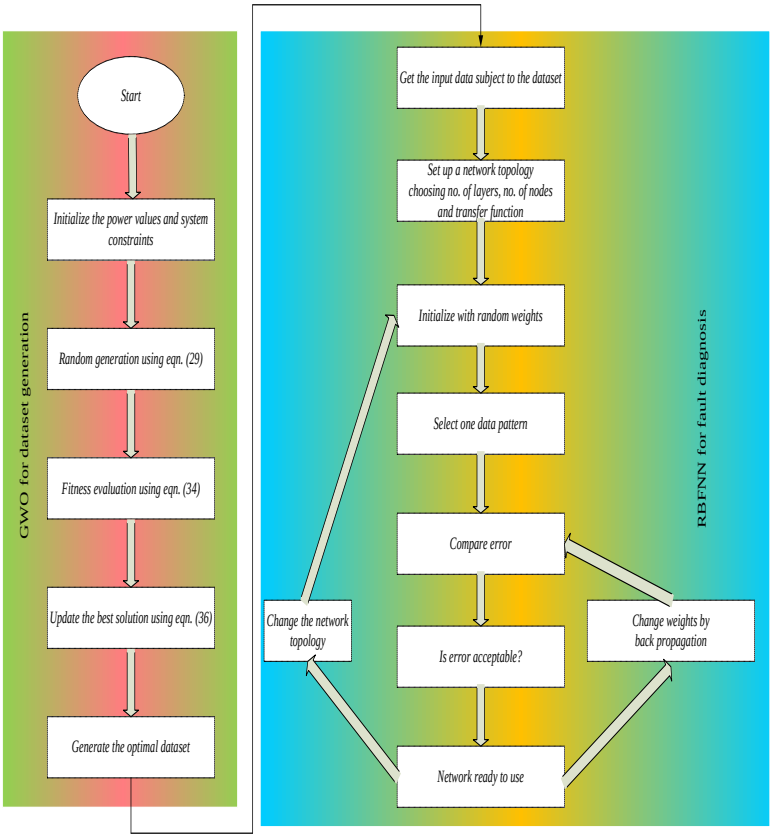

Figure 7: Flowchart of the proposed GWO-RBFNN approach

Step 5: This step used to minimize the BPR by reiterating the process from Step 2 until the smallest error value is reached [37].

$$10\,SE_{BP}^{k} < 1 \qquad (43)$$

Once the above-formulated steps are successfully completed, the RBFNN is ready to diagnose the healthy and unhealthy signals of the motor based on the error value. Finally, by utilizing the proposed optimization strategy, it can provide the optimal control of IM.

5. Simulation Results and Discussions

In this section, the effectiveness and the performance of the proposed method are described subject to the inter-turn insulation fault detection and diagnosis using the GWO-RBFNN technique. In this paper, the generation of fault datasets and the diagnosis of inter-turn insulation fault are done by the proposed GWO and the RBFNN technique. The developed model of the IM is simulated under the healthy and unhealthy (inter-turn insulation fault) conditions (10% shorted turns) with a balanced three-phase power supply. The

simulation results obtained from the proposed approach are compared with the existing techniques such as combined strategy of salp swarm optimization and recurrent neural network (CSSRN), Adaptive Neuro-Fuzzy Interference System (ANFIS) [38, 39], Recurrent Neural Network (RNN) [40, 41, 42], and Salp Swarm Algorithm with Artificial Neural Network (SSAANN) strategies. The proposed GWO-RBFNN technique is executed in the MATLAB/Simulink working platform. The proposed work is carried out on an Intel Core2 Quad CPU Q6600 at 2.40 GHz computer with 2 GB random access memory. The test experiments are analyzed by using the MATLAB R2013a (8.1.0.604) 32-bit and Version 3.7.2.

5.1. Simulation results for a healthy motor

This section describes the simulation results of the IM with no inter-turn insulation fault (unshorted turns) which is illustrated in figure 8 and this figure consolidates the pu developed stator current, stator voltages, and torque. The subplot 8(a) illustrates the pu current of the stator which generates the maximum of 1 A current between the time intervals 0-0.02 sec after that, the generated current is balanced till the end of the operation. The pu voltages of the stator in d-axis and q-axis are shown in subplot 8(b-c) and the maximum generated stator voltages are greater than 0.05 Vin both the axis. The subplot 8(d) illustrates the pu developed torque which generates the maximum of 0.005 Te. All the above-mentioned current, voltages and the torque of the stator winding in IM is generated between the time intervals of 0-0.2 sec. In this normal condition, all the current, voltages and torque are balanced and unity.

5.2. Simulation Results for an Unhealthy Motor

This section describes the simulation results of the IM with inter-turn insulation fault (shorted turn) of phase ‘A’, phase ‘B’, phase ‘c’, phase ‘AB’, phase ‘BC’ and phase ‘ABC’ of the stator winding. In the shorted turn faulty condition, the winding function of the injured phase is changed when an inter-turn short circuit arises. During the occurrence of an inter-turn insulation fault, the winding function of the injured phase ‘A’ is illustrated in figure 9 and this figure consolidates the pu developed stator current, stator voltages and torque of phase ‘A’ stator winding of IM. The subplot 9(a) illustrates the three-phase stator current under inter-turn insulation fault. The same figure shows that the inter-turn fault is generated between the time intervals of 0.09-0.12 sec after that it remains balanced. In this plot, the maximum generated current is 0.5 A. The subplot 9(b-c) illustrates the stator voltage in d-axis and q-axis under inter-turn insulation fault. As seen from this plot, the voltage signals are disturbed between the time intervals of 0.09-0.11 sec after that it remains balanced. The maximum voltages generated in the d and q-axis is greater than 0.05 V. The pu developed torque of the stator winding under faulty condition is shown in subplot 9(d). The winding function of the injured phase ‘B’ is illustrated in figure 10 and this figure consolidates the pu developed stator current, stator voltages, and torque of phase ‘B’ of the stator winding in IM. The subplot 10(a) illustrates the three-phase stator current under inter-turn insulation fault. The same figure shows that the inter-turn fault is generated between the time intervals of 0.09-0.12 sec after that it remains balanced. In this plot, the maximum generated current is 1 A. The subplot 10(b-c) illustrates the stator voltage in d-axis and q-axis under inter-turn insulation fault. As seen from this plot, the voltage signals are disturbed between the time intervals of 0.09-0.11 sec after that it remains balanced. The maximum voltages in d and q-axis are greater than 0.05 V, both the voltage signals are balanced and unity after the particular time period. The pu developed torque of the stator winding under faulty condition is shown in subplot 10(d). Initially, the peak level of the torque is less than 0.01 Te after that it is reduced.

The winding function of the injured phase ‘C’ during the inter-turn insulation fault is illustrated in figure 11 which includes the pu developed stator current, stator voltages and torque of phase ‘C’ in the stator winding of IM. The subplot 11(a) illustrates the three-phase stator current phase ‘C’. Initially, the fault is generated between the time intervals of 0-0.03 sec after that it is balanced till 0.08 sec. Again the inter-turn fault is generated between the time intervals of 0.08-0.13 sec after that it remains balanced. In this plot, the maximum generated current is 1 A. The subplot 11(b-c) illustrates the stator voltage in d-axis and q-axis under inter-turn insulation fault. As seen from this plot, from the time period of 0-0.09 sec, the signal is balanced and unity after that the voltage signals are disturbed between the time intervals of 0.09-0.12 sec then it remains balanced till the end of the operation. The maximum voltages generated in the d and q-axis is greater than 0.05 V. The pu developed torque of the stator winding under faulty condition is shown in subplot 11(d). The winding function of the injured phase ‘AB’ is illustrated in figure 12 and this figure consolidates the pu developed stator current, stator voltages and torque of phase ‘AB’ in the stator winding of IM. The subplot 12(a) illustrates the three-phase stator current under shorted turn fault. This figure shows that the inter-turn fault is generated between the time intervals of 0.09-0.13 sec after that it remains balanced. In this plot, the maximum generated current is 1 A. The subplot 12(b-c) illustrates the stator voltage in d-axis and q-axis under inter-turn insulation fault. Initially, the voltage is balanced and unity till 0.09 sec after that it is disturbed up to 0.12 sec then the signal remains balanced and unity till the end of the operation.

The pu developed torque of the stator winding in phase 'AB' is shown in subplot 12(d). Initially, the peak level of the torque is 0.005 Te after that it is reduced and remains constant till the end of the operation.

The winding function of the injured phase 'BC' during the inter-turn insulation fault is illustrated in figure 13 which includes the pu developed stator current, stator voltages and torque of phase 'C' in the stator winding of IM. The subplot 13(a) illustrates the three-phase stator current phase 'BC'. Initially, the 'BC' phase fault is generated between the time intervals of 0-0.01 sec after that it is balanced till 0.08 sec. Again the fault is generated from 0.08-0.13 sec after that it remains balanced. In this plot, the maximum generated current is greater than 1 A. The subplot 13(b-c) illustrates the stator voltage in d-axis and q-axis under inter-turn insulation fault. In this plot, the signal is balanced and unity between the time periods of 0-0.09 sec after that the voltage signals are disturbed till 0.12 sec then it remains balanced till the end of the operation. The maximum voltages generated in the d and q-axis is greater than 0.05 V. The pu developed torque of the stator winding under the faulty condition in phase 'BC' is shown in subplot 13(d) and the maximum level of the torque is 0.005 Te. The winding function of the injured phase 'ABC' is illustrated in figure 14 and this figure consolidates the pu developed stator current, stator voltages and torque of phase 'ABC' in the stator winding of IM. In subplot 14(a), the stator fault is generated between the time intervals of 0.08-0.13 sec. In subplot 14(b) and 14(c), the fault is generated between the time intervals of 0.08-0.12 sec. The pu developed torque of the stator winding in phase 'ABC' is shown in subplot 14(d). The maximum torque level is 0.005 Te after that it is reduced and remains constant till the end of the operation.

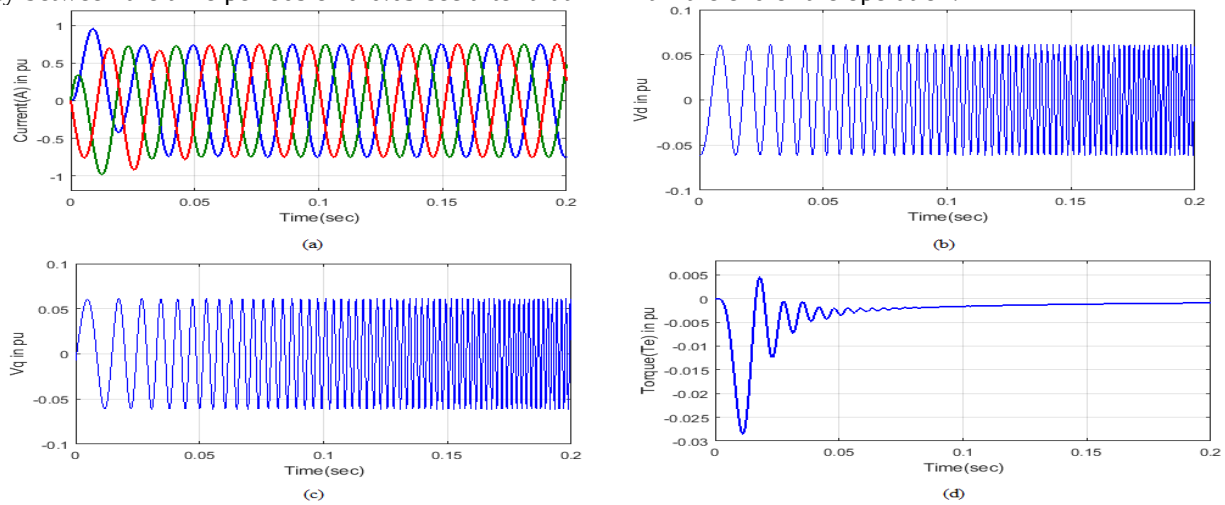

Figure 8: Simulation results of the IM with unshorted turns (a) Stator current (b) Stator voltage Vd (c) Stator voltage Vq (d) Torque

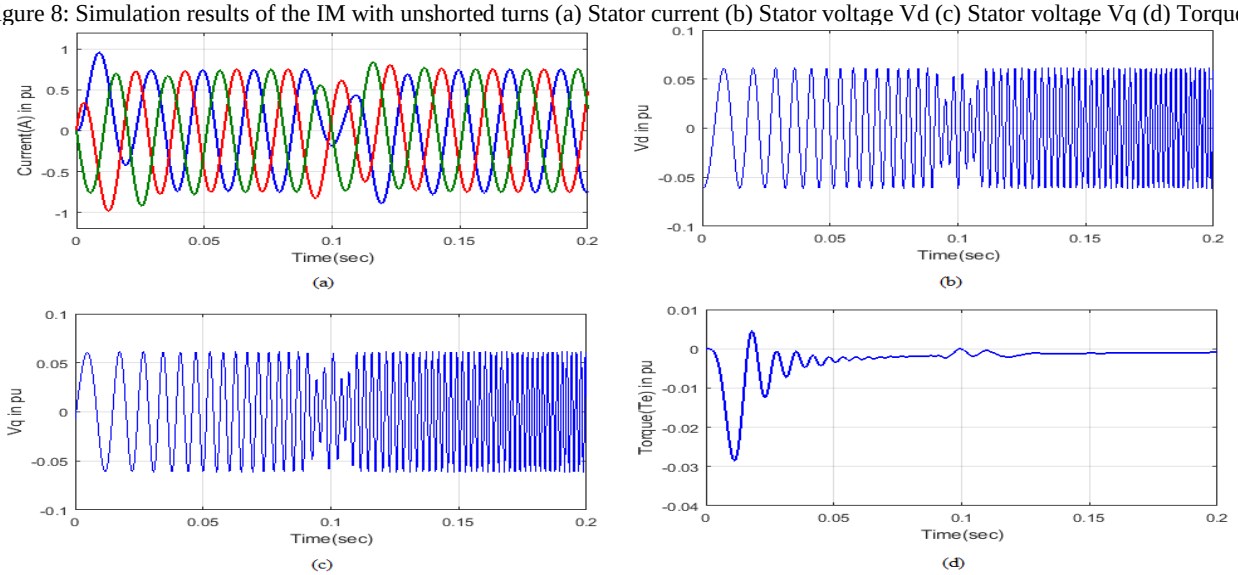

Figure 9: Simulation results of the IM with inter-turn insulation fault in phase 'A' (a) Stator current (b) Stator voltage Vd (c) Stator voltage Vq (d) Torque

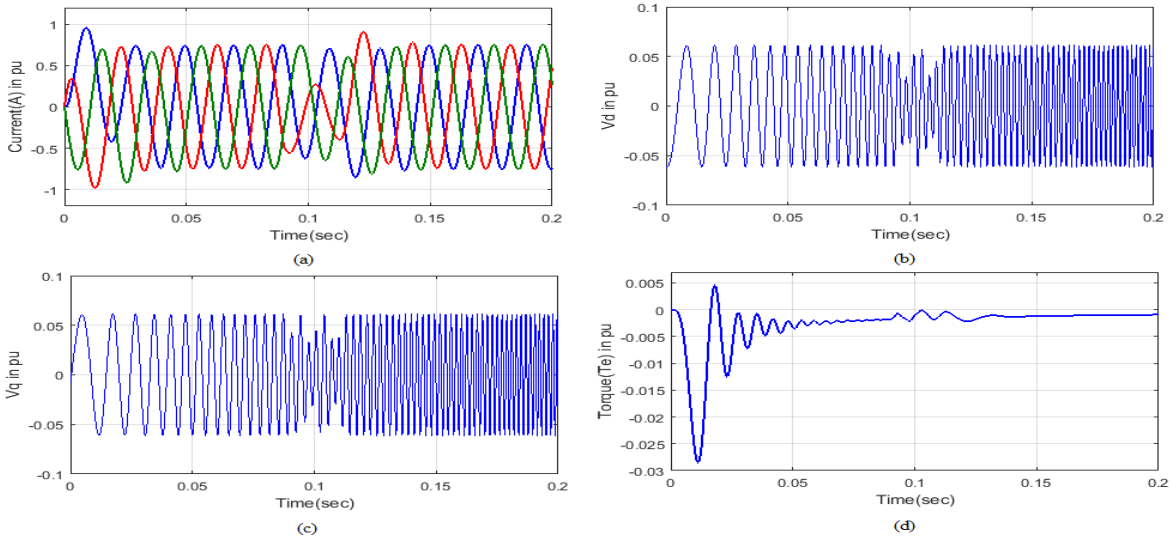

Figure 10: Simulation results of the IM with inter-turn insulation fault in phase 'B' (a) Stator current (b) Stator voltage Vd (c) Stator voltage Vq (d) Torque

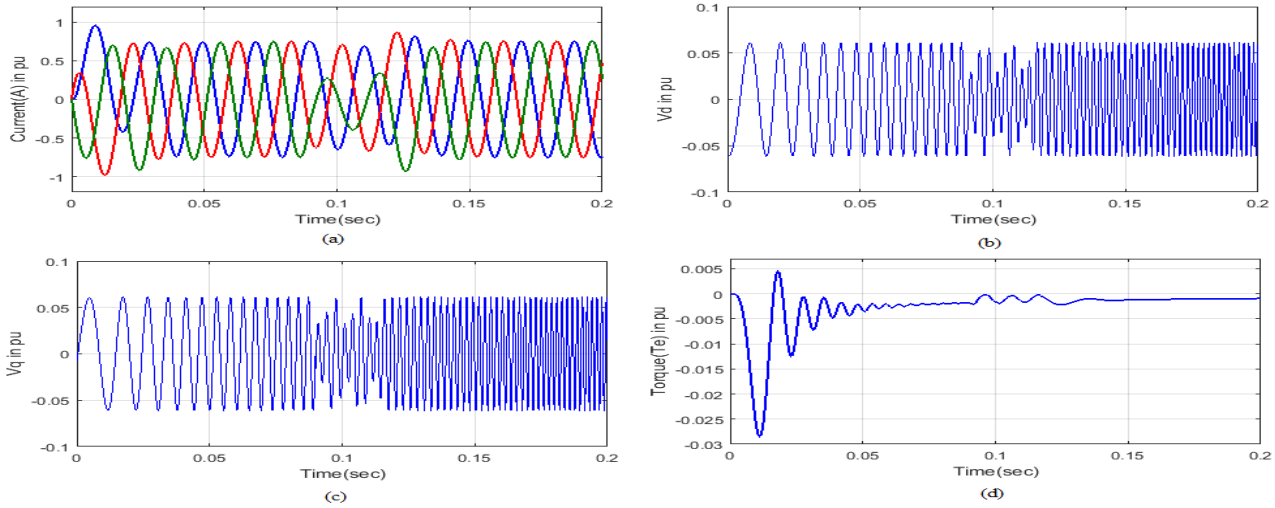

Figure 11: Simulation results of the IM with inter-turn insulation fault in phase 'C' (a) Stator current (b) Stator voltage Vd (c) Stator voltage Vq (d)

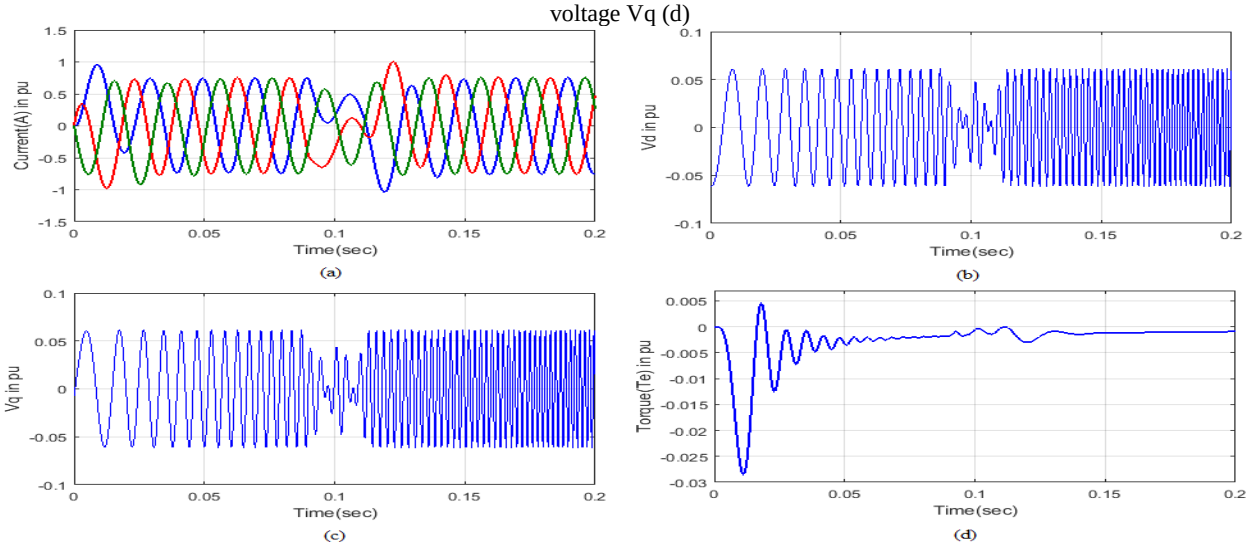

Figure 12: Simulation results of the IM with inter-turn insulation fault in phase 'AB' (a) Stator current (b) Stator voltage Vd (c) Stator voltage Vq (d) Torque

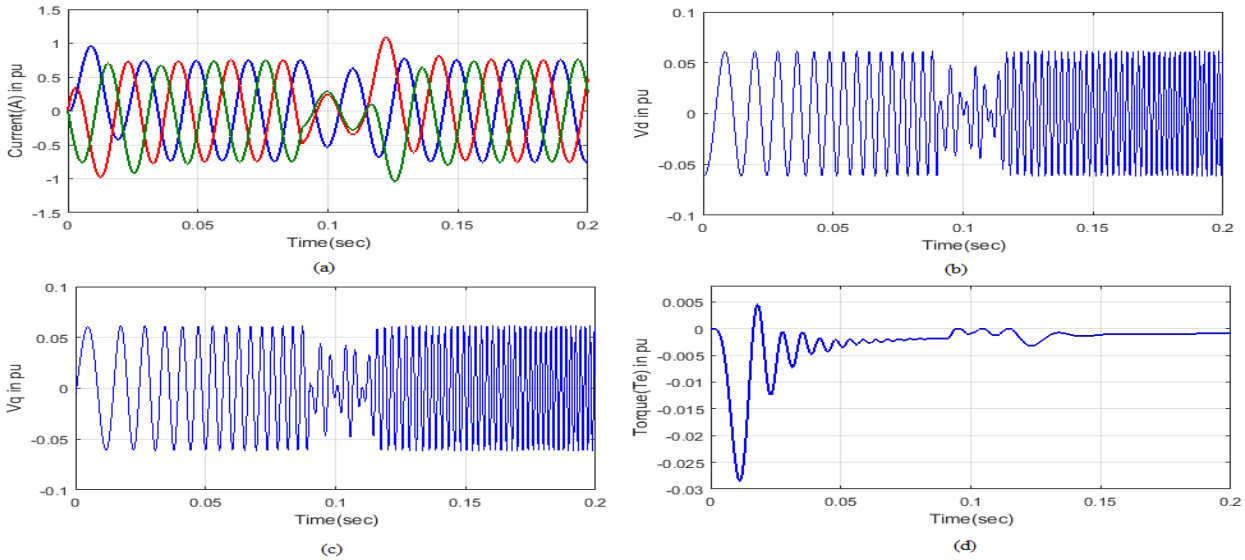

Figure 13: Simulation results of the IM with inter-turn insulation fault in phase 'BC' (a) Stator current (b) Stator voltage Vd (c) Stator voltage Vq (d) Torque

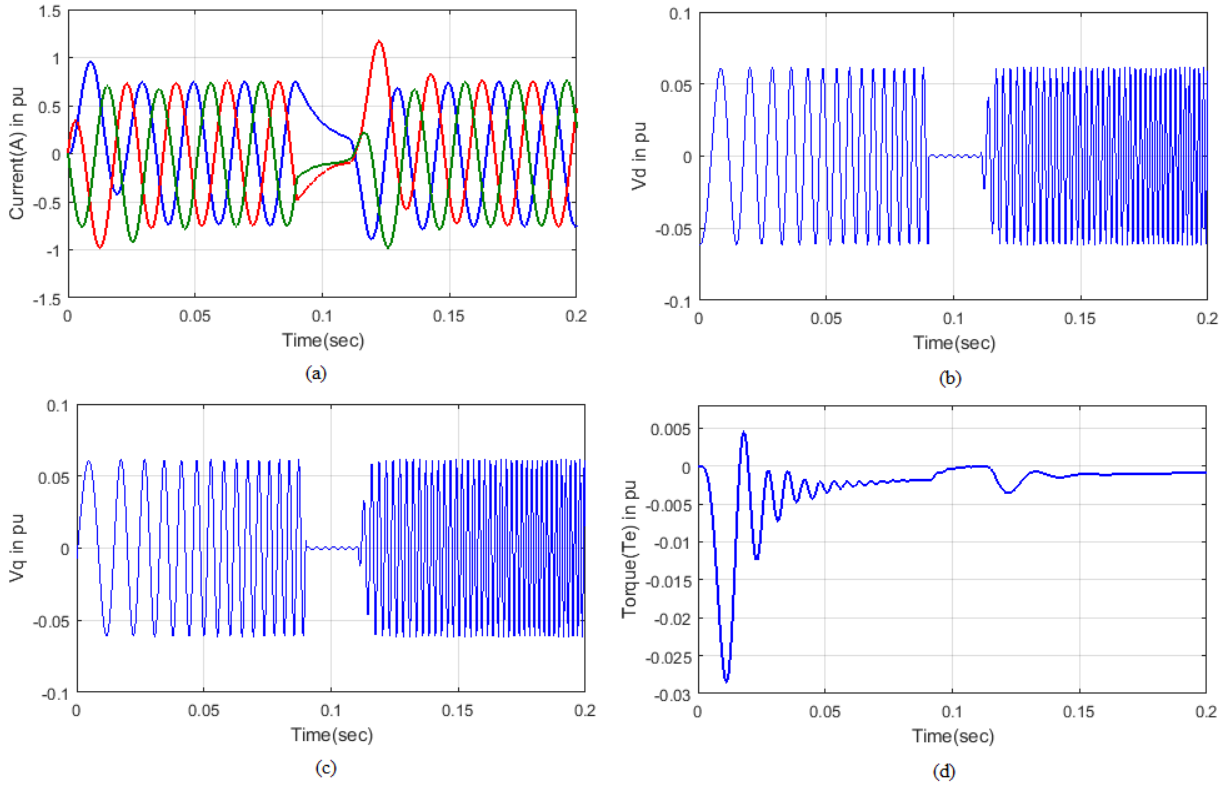

Figure 14: Simulation results of the IM with inter-turn insulation fault in phase 'ABC' (a) Stator current (b) Stator voltage Vd (c) Stator voltage Vq (d) Torque

5.3. Performance Analysis

This section analyses the performances of the proposed GWO-RBFNN approach which is compared with the existing techniques such as CSSRN, ANFIS, RNN, and SSAANN approaches to analyze the effective approach. To analyze the performance, the classification process is done subject to the true positive (TP), true negative (TN), false positive (FP) and false negative (FN) classes. The correctly labeled positive signals are known as TP. The correctly labeled negative signals are known as TN. The incorrectly labeled negative signals are known as FP. The incorrectly labeled positive signals are known as FN. The performance measures are utilized to evaluate the diagnosis results and they are computed as follows,

$$Accuracy = \frac{TP + TN}{TP + TN + FP + FN} \quad (44)$$

$$\text{Pr}ecision = \frac{TP}{TP + FP} \quad (45)$$

$$\text{Re}call \ (or) \ specificity = \frac{TP}{TP + FN} \quad (46)$$

$$Sensitivity = \frac{TN}{TN + FP} \quad (47)$$

In the above equation, if the sensitivity value is positive, (i.e.) true positive fraction, the inter-turn insulation fault occurs in the stator winding of the IM. If the specificity value is negative, (i.e.) true negative fraction that means the IM is in a healthy condition.

Table 1: Performance comparison of proposed with existing method during inter-turn insulation fault for 50 and 100 number of trials

Performance Measures	50 trials				
	ANFIS	RNN	SSAANN	CSSRN	Proposed
Accuracy	0.55	0.75	0.85	0.95	0.98
Specificity	0.5	0.7	0.8	0.9	0.94
Recall	0.6	0.8	0.9	1	1.53
Precision	0.52	0.72	0.82	0.9	0.96
	100 trials				
Accuracy	0.6	0.7	0.8	0.9	0.93
Specificity	0.53	0.63	0.75	0.85	0.9
Recall	0.57	0.6	0.85	0.8	0.85
Precision	0.55	0.65	0.72	0.95	0.98

The performance comparison of proposed with existing method during inter-turn insulation fault for 50 and 100 number of trials are delineated in Table 1 which includes the accuracy, specificity, recall, and precision. In 50 number of trials, the proposed method has the accuracy is 0.98, specificity is 0.94, recall is 1.53 and the precision is 0.9. In the above mentioned existing method, the accuracy, specificity, recall and the precision ranges in ANFIS are 0.55, 0.5, 0.6 and 0.52 respectively. In RNN, the ranges are 0.75, 0.7, 0.8 and 0.82 respectively. In SSAANN, the ranges in accuracy, specificity, recall, and precision are 0.85, 0.8, 0.9 and 0.82 respectively. In CSSRN, the ranges in accuracy, specificity, recall, and precision are 0.95, 0.9, 0.1 and 0.9 respectively. In 100 number of trials, the proposed method has the accuracy is 0.93, specificity is 0.9, recall is 1.85 and the precision is 0.98. In the above mentioned existing method, the accuracy, specificity, recall and the precision ranges in ANFIS are 0.6, 0.53, 0.57 and 0.55 respectively. In RNN, the ranges are 0.7, 0.63, 0.6 and 0.65 respectively. In SSAANN, the ranges in accuracy, specificity, recall, and precision are 0.8, 0.75, 0.85 and 0.72 respectively. In CSSRN, the ranges in accuracy, specificity, recall, and precision are 0.9, 0.85, 0.8 and 0.95 respectively. Compared with the above mentioned existing method, the proposed method performs very precisely and accurately.

5.4. Statistical Evaluation

In order to evaluate the overall system performance the statistical measures such as (1) Root Mean Square Error (RMSE), Mean Absolute Percentage Error (MAPE) and Mean Bias Error (MBE) are computed. The overall classification efficiency of the proposed method is estimated subject to the error metric RMSE. A large deviation occurs in the diagnosis from the target value when the RMSE value is large. Likewise, the MBE error computation is used to estimate the average deviation of the system. The diagnosis is under forecasted when the value of the MBE is negative. As well as, the accuracy of the overall system is computed subject to the MAPE value. These error metrics are computed as follows,

$$RMSE = \sqrt{\frac{\sum_{m=1}^{Z} (N_{tar}^{k} - N_{out}^{k})}{Z}} \quad (48)$$

$$MAPE = \frac{1}{Z} \sum_{m=1}^{Z} \left| \frac{N_{tar}^{k} - N_{out}^{k}}{N_{tar}^{k}} \right| a \quad (49)$$

$$MBE = \frac{1}{Z} \sum_{m=1}^{Z} N_{out}^{k} - N_{tar}^{k} \quad (50)$$

Where N_{tar}^{k} is represents the target value, N_{out}^{k} represents the detected value, a is represents a number of samples per leaf, Z is the total number of samples.

Table 2: Statistical comparison of proposed with existing method during turn insulation fault for 50 and 100 number of trials

Metrics	50 trials				
	ANFIS	RNN	SSAANN	CSSRN	Proposed
RMSE	26.4	18.9	23.5	10.3	8.25
MAPE	17.2	6.4	13.0	1	0.97
MBE	7.1	2.9	5.1	2.7	1.37
Consumption time (s)	7.8	6.5	8.0	5.2	2.96
	100 trials				
RMSE	29.4	21.9	26.5	13.5	9.38
MAPE	18.2	7.4	14.0	2	1.91
MBE	10.1	5.9	8.1	5.7	3.87
Consumption time (s)	8	7	8.3	6	2.98

Table 2 shows the statistical analysis of the proposed method. Here, to evaluate the overall performance of the proposed method, the proposed GWO-RBFNN fault diagnosis approach is compared with the existing well-known classification approaches such as ANFIS, RNN, SSAANN, and CSSRN. In 50 number of trials, The RMSE, MAPE and the MBE range of the proposed method is 8.25 %, 0.97 %, 1.37 % and the time consumption of the proposed method are 2.96 (s). In 100 number of trials, The RMSE, MAPE and the MBE

range of the proposed method is 9.38 %, 1.91 %, 3.87 % and the time consumption of the proposed method are 2.98 (s). Compared with the existing approaches the proposed method has less error and very less amount of consumption time.

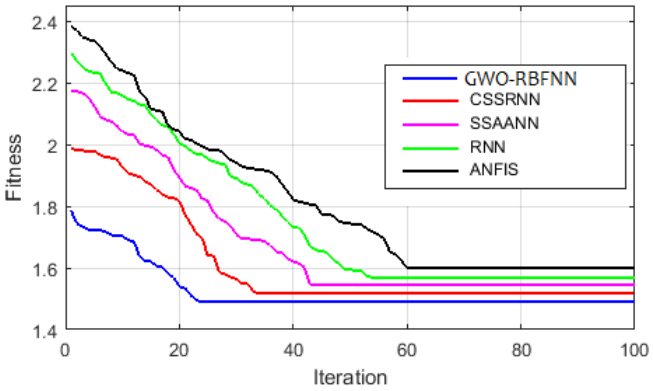

Figure 15: Fitness comparison of the proposed and the existing approaches

Figure 15 shows the fitness of the proposed GWO-RBFNN method which is compared with the existing technologies such as CSSRNN, SSAANN, RNN and ANFIS. The fitness is executed subject to the equation (34). Here, which technique has the minimum fitness is considered as the best technique. As per this, the proposed method has the minimum fitness (1.8) when compared with the other techniques. As seen from this, the proposed method performs very well to detect and classify the stator inter-turn insulation fault in the IM.

6. Conclusions

This paper presents a hybridized GWO-RBFNN based detection and diagnosis method for inter-turn insulation fault detection in the three-phase IM. In the proposed approach, the detection and classification of stator inter-turn insulation fault are the main two stages. The optimal dataset is generated by the GWO approach as well as the shorted and the unshorted turns are classified by the RBFNN technique. The simulation analysis of the proposed method is tested under the healthy and unhealthy conditions of the motor. Utilizing performance measures such as accuracy, precision, recall, specificity and the statistical measures such as RMSE, MAPE, MBE and consumption time, the execution of the proposed technique is authenticated and in addition, the proposed technique is compared with existing technologies such as ANFIS, RNN, CSSRN, and SSAANN techniques. The result obtained from the simulation analysis shows that the extreme occurrence of an inter-turn fault in the distribution system is detected accurately with the new optimal technique by utilizing the proposed methodology. Also, the proposed technique is effective to classify the inter-turn fault with less computation and reduces the complexity of the algorithm.

References

1. S. Nandi, H. Toliyat and X. Li, *Condition Monitoring and Fault Diagnosis of Electrical Motors—A Review*, IEEE Transactions on Energy Conversion, vol. 20, no. 4, pp. 719-729, 2005.
2. M. Haji and H. Toliyat, *Pattern recognition-a technique for induction machines rotor broken bar detection*, IEEE Transactions on Energy Conversion, vol. 16, no. 4, pp. 312-317, 2001.
3. M. Seera, Chee Peng Lim, D. Ishak and H. Singh, *Fault Detection and Diagnosis of Induction Motors Using Motor Current Signature Analysis and a Hybrid FMM–CART Model*, IEEE Transactions on Neural Networks and Learning Systems, vol. 23, no. 1, pp. 97-108, 2012.
4. L. Eren and M. Devaney, *Bearing Damage Detection via Wavelet Packet Decomposition of the Stator Current*, IEEE Transactions on Instrumentation and Measurement, vol. 53, no. 2, pp. 431-436, 2004.
5. B. Mirafzal and N. Demerdash, *On innovative methods of induction motor interturn and broken-bar fault diagnostics*, IEEE Transactions on Industry Applications, vol. 42, no. 2, pp. 405-414, 2006.
6. D. Karaboga and E. Kaya, *Adaptive network based fuzzy inference system (ANFIS) training approaches: a comprehensive survey*, Artificial Intelligence Review, 2018.
7. M. Ballal, Z. Khan, H. Suryawanshi and R. Sonolikar, *Adaptive Neural Fuzzy Inference System for the Detection of Inter-Turn Insulation and Bearing Wear Faults in Induction Motor*, IEEE Transactions on Industrial Electronics, vol. 54, no. 1, pp. 250-258, 2007.
8. F. Zidani, D. Diallo, M. Benbouzid and R. Nait-Said, *A Fuzzy-Based Approach for the Diagnosis of Fault Modes in a Voltage-Fed PWM Inverter Induction Motor Drive*, IEEE Transactions on Industrial Electronics, vol. 55, no. 2, pp. 586-593, 2008.
9. G. Joksimovic and J. Penman, *The detection of inter-turn short circuits in the stator windings of operating motors*, IEEE Transactions on Industrial Electronics, vol. 47, no. 5, pp. 1078-1084, 2000.
10. A. Gandhi, T. Corrigan and L. Parsa, *Recent Advances in Modeling and Online Detection of Stator Interturn Faults in Electrical Motors*, IEEE Transactions on Industrial Electronics, vol. 58, no. 5, pp. 1564-1575, 2011.
11. A. Stavrou, H. Sedding and J. Penman, *Current monitoring for detecting inter-turn short circuits in induction motors*, IEEE Transactions on Energy Conversion, vol. 16, no. 1, pp. 32-37, 2001.
12. M. Bouzid, G. Champenois, N. Bellaaj, L. Signac and K. Jelassi, *An Effective Neural Approach for the Automatic Location of Stator Interturn Faults in Induction Motor*, IEEE Transactions on Industrial Electronics, vol. 55, no. 12, pp. 4277-4289, 2008.
13. P. Jover Rodríguez and A. Arkkio, *Detection of stator winding fault in induction motor using fuzzy logic*, Applied Soft Computing, vol. 8, no. 2, pp. 1112-1120, 2008.
14. D. Shah, S. Nandi and P. Neti, *Stator-Interturn-Fault Detection of Doubly Fed Induction Generators Using Rotor-Current and Search-Coil-Voltage Signature Analysis*, IEEE Transactions on Industry Applications, vol. 45, no. 5, pp. 1831-1842, 2009.
15. C. De Angelo, G. Bossio, S. Giaccone, M. Valla, J. Solsona and G. Garcia, *Online Model-Based Stator-Fault Detection and Identification in Induction Motors*, IEEE Transactions on Industrial Electronics, vol. 56, no. 11, pp. 4671-4680, 2009.

16. I. Önel and M. Benbouzid, *Induction Motor Bearing Failure Detection and Diagnosis: Park and Concordia Transform Approaches Comparative Study*, IEEE/ASME Transactions on Mechatronics, vol. 13, no. 2, pp. 257-262, 2008.
17. R. Sharifi and M. Ebrahimi, *Detection of stator winding faults in induction motors using three-phase current monitoring*, ISA Transactions, vol. 50, no. 1, pp. 14-20, 2011.
18. H. Henao, H. Razik and G. Capolino, *Analytical Approach of the Stator Current Frequency Harmonics Computation for Detection of Induction Machine Rotor Faults*, IEEE Transactions on Industry Applications, vol. 41, no. 3, pp. 801-807, 2005.
19. V. Ghate and S. Dudul, *Optimal MLP neural network classifier for fault detection of three phase induction motor*, Expert Systems with Applications, vol. 37, no. 4, pp. 3468-3481, 2010.
20. Sang Bin Lee, R. Tallam and T. Habetler, *A robust, on-line turn-fault detection technique for induction machines based on monitoring the sequence component impedance matrix*, IEEE Transactions on Power Electronics, vol. 18, no. 3, pp. 865-872, 2003.
21. M. Ali, M. Shabbir, X. Liang, Y. Zhang and T. Hu, *Machine Learning based Fault Diagnosis for Single- and Multi-Faults in Induction Motors Using Measured Stator Currents and Vibration Signals*, IEEE Transactions on Industry Applications, pp. 1-1, 2019.
22. V. Boorgula and S. Tulasi Ram, *Incipient Fault Diagnosis in Stator Winding of Synchronous Generator: A CMFFLC Technique*, IETE Journal of Research, pp. 1-12, 2018.
23. E. Elbouchikhi, Y. Amirat, G. Feld and M. Benbouzid, *Generalized Likelihood Ratio Test-based Approach for Stator Faults Detection in a PWM Inverter-Fed Induction Motor Drive*, IEEE Transactions on Industrial Electronics, pp. 1-1, 2018.
24. L. Maraaba, Z. Al-Hamouz and M. Abido, *An Efficient Stator Inter-Turn Fault Diagnosis Tool for Induction Motors*, Energies, vol. 11, no. 3, p. 653, 2018.
25. P. Rebouças Filho, N. Nascimento, I. Sousa, C. Medeiros and V. de Albuquerque, *A reliable approach for detection of incipient faults of short-circuits in induction generators using machine learning*, Computers & Electrical Engineering, vol. 71, pp. 440-451, 2018.
26. G. Surya, Z. Khan, M. Ballal and H. Suryawanshi, *A Simplified Frequency-Domain Detection of Stator Turn Fault in Squirrel-Cage Induction Motors Using an Observer Coil Technique*, IEEE Transactions on Industrial Electronics, vol. 64, no. 2, pp. 1495-1506, 2017.
27. Xiaogang Luo, Yuefeng Liao, H. Toliyat, A. El-Antably and T. Lipo, *Multiple coupled circuit modeling of induction machines*, IEEE Transactions on Industry Applications, vol. 31, no. 2, pp. 311-318, 1995.
28. J. Gojko, D. Momir and O. Aleksandar, *Skew and linear rise of MMF across slot modelling-winding function approach*, IEEE Transactions on Energy Conversion, vol. 14, no. 3, pp. 315-320, 1999.
29. S. Mirjalili, S. Mirjalili and A. Lewis, *Grey Wolf Optimizer*, Advances in Engineering Software, vol. 69, pp. 46-61, 2014.
30. E. Emary, H. Zawbaa and A. Hassanien, *Binary grey wolf optimization approaches for feature selection*, Neurocomputing, vol. 172, pp. 371-381, 2016.
31. S. Mirjalili, S. Saremi, S. Mirjalili and L. Coelho, *Multi-objective grey wolf optimizer: A novel algorithm for multi-criterion optimization*, Expert Systems with Applications, vol. 47, pp. 106-119, 2016.
32. M. Kohli and S. Arora, *Chaotic grey wolf optimization algorithm for constrained optimization problems*, Journal of Computational Design and Engineering, vol. 5, no. 4, pp. 458-472, 2018.
33. M. Shakarami and I. Faraji Davoudkhani, *Wide-area power system stabilizer design based on Grey Wolf Optimization algorithm considering the time delay*, Electric Power Systems Research, vol. 133, pp. 149-159, 2016.
34. H. Baghaee, M. Mirsalim, G. Gharehpetan and H. Talebi, *Nonlinear Load Sharing and Voltage Compensation of Microgrids Based on Harmonic Power-Flow Calculations Using Radial Basis Function Neural Networks*, IEEE Systems Journal, vol. 12, no. 3, pp. 2749-2759, 2018.
35. M. Halali, V. Azari, M. Arabloo, A. Mohammadi and A. Bahadori, *Application of a radial basis function neural network to estimate pressure gradient in water–oil pipelines*, Journal of the Taiwan Institute of Chemical Engineers, vol. 58, pp. 189-202, 2016.
36. C. Sbarufatti, M. Corbetta, M. Giglio and F. Cadini, *Adaptive prognosis of lithium-ion batteries based on the combination of particle filters and radial basis function neural networks*, Journal of Power Sources, vol. 344, pp. 128-140, 2017.
37. A. Rubio-Solis and G. Panoutsos, *Interval Type-2 Radial Basis Function Neural Network: A Modeling Framework*, IEEE Transactions on Fuzzy Systems, vol. 23, no. 2, pp. 457-473, 2015. Available: 10.1109/tfuzz.2014.2315656.
38. V. Selvara, *Adaptive Neuro Fuzzy Inference Systems Based Clustering Approach For Wireless Sensor Networks*, International Journal of Engineering and Computer Science, vol. 6, no. 11, 2017.
39. A. Nürnberger, D. Nauck and R. Kruse, *Neuro-fuzzy control based on the NEFCON-model: recent developments*, Soft Computing - A Fusion of Foundations, Methodologies and Applications, vol. 2, no. 4, pp. 168-182, 1999.
40. E. Yadegaridehkordi, M. Nilashi, M. Nasir and O. Ibrahim, *Predicting determinants of hotel success and development using Structural Equation Modelling (SEM)-ANFIS method*, Tourism Management, vol. 66, pp. 364-386, 2018.
41. L. Zhang, Z. Yi and S. Amari, *Theoretical Study of Oscillator Neurons in Recurrent Neural Networks*, IEEE Transactions on Neural Networks and Learning Systems, pp. 1-7, 2018.
42. R. Selva Santhose Kumar and S. Girirajkumar, *Z-Source Inverter Fed Induction Motor Drive control using Particle Swarm Optimization Recurrent Neural Network*, Journal of Intelligent & Fuzzy Systems, vol. 28, no. 6, pp. 2749-2760, 2015.